Journal of Cleaner Production 274 (2020) 122487

Contents lists available at ScienceDirect

Journal of Cleaner Production

journal homepage: www.elsevier.com/locate/jclepro

Characterizing urbanization-induced land surface phenology change from time-series remotely sensed images at fine spatio-temporal scale: A case study in Nanjing, China (2001–2018)

Xin Wang [a, b, c, e], Peijun Du [a, b, c, d, *], Dongmei Chen [e], Cong Lin [a, b, c, d], Hongrui Zheng [a, b, c, d], Shanchuan Guo [a, b, c, d]

[a] School of Geography and Ocean Science, Nanjing University, Nanjing, Jiangsu, 210023, China
[b] Key Laboratory for Land Satellite Remote Sensing Applications of Ministry of Natural Resources, Nanjing, Jiangsu, 210023, China
[c] Jiangsu Provincial Key Laboratory of Geographic Information Science and Technology, Nanjing, Jiangsu, 210023, China
[d] Jiangsu Center for Collaborative Innovation in Geographical Information Resource Development and Application, Nanjing, Jiangsu, 210023, China
[e] Department of Geography and Planning, Queen's University, Kingston, ON, K7L 3N6, Canada

ARTICLE INFO

Article history:
Received 25 December 2019
Received in revised form
12 March 2020
Accepted 23 May 2020
Available online 17 July 2020

Handling editor: Yutao Wang

Keywords:
Urbanization
Impervious surface
Ensemble continuous change detection and classification
Land surface phenology
Landsat
MODIS

ABSTRACT

Continuous urban expansion and its influence on land surface phenology (LSP) have been gaining considerable attention due to their impacts on climate change, carbon cycling and human health. Most previous studies have investigated the effects of urbanization on LSP from the regional to global scales by using coarse-resolution remotely sensed images and fixed land cover boundary maps. However, the influences of urbanization on LSP are also important at the local level, particularly in and around rapidly urbanizing cities as LSP is closely linked to the local ecology and people's health. To analyze the dynamic of urbanization and its effect on LSP at the local scale, this study proposed a novel framework of characterizing LSP with consideration of continuous urban expansion based on all available time-series Landsat and Moderate Resolution Image Spectroradiometer (MODIS) Reflectance and Enhanced Vegetation Index (EVI) composite data. The proposed approach was capable of evaluating LSP impacts of urbanization from three aspects: 1) the phenology difference between dynamic annual urban and rural areas; 2) the different rates of phenology trend between the permanent urban and rural areas; and 3) the phenology shifts in the areas that were urbanized during the period. This approach was applied to Nanjing, China and the experimental results indicated that when compared with the rural areas, the phenology cycle started 0.59 ± 0.58 days earlier (start of season, SOS) and ended 1.65 ± 1.55 days later (end of season, EOS) in urban areas, accordingly leading to increased growing season length (GSL) by 2.77 ± 2.61 days. Besides, the experiments also revealed that 70.81% SOS and 78.79% EOS in the permanent urban-rural areas were provided with delayed phenology trends, along with 80.72% of these regions tending to have a prolonged GSL. Furthermore, the rates of SOS and EOS delay in rural areas were 0.12 ± 0.12 day/year and 0.02 ± 0.02 day/year faster than those in urban areas, and the rate of GSL prolonging in urban regions was 0.04 ± 0.04 day/year faster than that in rural counterparts. For the urbanized regions in Nanjing, after experiencing conversion to the impervious surface, SOS and EOS delayed in 65.77% and 70.33% of the regions, accompanied by extended GSL in 70.83% of the regions. Overall, this research proposed a novel approach of analyzing urbanization implications for LSP at the city scale and demonstrated its priority of taking continuous land cover change into account.

1. Introduction

The terrestrial surface has been heavily modified under the situation of rapid economic development and population growth. The rapid increase of the urban population due to migration from rural areas is the key factor of urban expansion (Zhang et al., 2019).

* Corresponding author. 163 Xianlin Avenue, Nanjing, China.
E-mail address: dupjrs@gmail.com (P. Du).

https://doi.org/10.1016/j.jclepro.2020.122487
0959-6526/

The increasing trend will lead the percentage of urban population to 70% by 2050, resulting in the global urban areas expanding much than ever by then (Feyisa et al., 2016). Urban areas tend to be provided with higher temperatures than the surrounding regions, referred to as urban heat island (UHI), mainly caused by the increasing of impervious surface at the expense of vegetation and evaporating soil which can reduce latent heat flux and increase sensible heat flux (Clinton and Gong, 2013). As a result, rapid and invasive urbanization not only depletes natural sources directly, but also affects surrounding land surface phenology (LSP), which in turn influences the local environmental and ecological processes including primary production (Imhoff et al., 2004), carbon and energy cycling (Hutyra et al., 2014; Wang et al., 2016), and flower pollination and seed set (Gaku et al., 2004). In addition, phenology changes also affect human health. For instance, prolonged growing season length (GSL) can lengthen the allergy seasons and thus increase the severity of allergies (Cecchi et al., 2010). Accurate knowledge of the process of urbanization and its implications for LSP, therefore, can not only help enhance understanding of the problems associated with increased urban area and population but also be essential for formulating mitigation strategies and ultimately build a sustainable city.

At present, the impacts of urbanization on LSP are not well understood. First of all, it is still inconclusive whether and to what extent urbanization influences LSP. Some studies observed advances of start of season (SOS), delays of end of season (EOS) and extensions of GSL in urban areas compared with the surrounding rural regions through field measurements of specific species (Lu et al., 2006; Roetzer et al., 2000) or remote sensing analysis for a large scale (regional or global) estimation with coarse spatial and temporal resolution data (Li et al., 2017; Zhang et al., 2004). In contrast, several studies demonstrated an insignificant difference or even a delay of SOS through the urbanization process (Gazal et al., 2008). Therefore, more accurate instance data with the finer spatio-temporal resolution are needed to reduce errors and uncertainties caused by missing data and mixed pixels. Second, global climate change has significant influences on phenology change (Piao et al., 2015), but the differences in its impacts on urbanized and rural areas are still unclear. Thus, with the background of global warming and fast urbanization condition, there is a strong impetus to better understand the difference of phenology trends throughout the past decades. Third, as mentioned before, urbanization comes at the expense of vegetated and other natural lands, resulting in abrupt phenology shifts, which also constitutes the phenology difference between urban and rural regions. However, their detailed changing properties and spatial distributions have not well studied.

Based on the results and issues summarized from the previous studies, continuous urban expansion and LSP with finer spatio-temporal resolution and comprehensive analysis of the relationship between these two elements are the key ways to achieve the solutions. Thus, the remainder of the paper is organized as follows. Section 2 presents the literature review to draw the state-of-the-art methods of obtaining and analyzing long-term urban expansion and LSP. Section 3 introduces the typical case study of Nanjing, where the urban area had expanded much during the period from 2001 to 2018. Section 4 illustrates the detailed strategy of calculating the extents of urban expansion, the dates of phenology indicators with the higher spatial and temporal resolution, and their spatio-temporal relationship. Section 5 displays the results and discoveries of the case study, followed by a discussion in Section 6. Finally, Section 7 concludes the study and puts forward some perspectives in the future.

2. Literature review

2.1. Monitoring continuous urban expansion

Impervious surface, which refers to the land cover type that prevents water filtration into the soil such as rooftops, sidewalks and paved roads (Arnold Jr and Gibbons, 1996), can not only reflect the process of urbanization but also indicate the environmental change from anthropogenic activity (Weng, 2012). With the expansion of impervious surfaces, numerous influences including changing of surface runoffs (Du et al., 2012; Miller et al., 2014), pollution from industrial emissions (Liang et al., 2019) and increasing temperature by UHI effect (Weng et al., 2004) have been revealed. Therefore, tracking impervious surface changes is a crucial step to understanding the process of urbanization and analyzing its implications for LSP. Monitoring impervious surface expansion is a change detection task that focuses on specific type of conversions, in which other land cover types transform to the impervious surface. Earth observation through remote sensing satellites can provide an effective and efficient way to capture repeated collection and monitor such dynamic changes in wide geographical areas (Ban et al., 2015; Liu et al., 2019). The developed change detection for impervious surface areas can be broadly categorized into pre-classification and post-classification methods (Singh, 1989). The pre-classification methods treat different types of land cover change as independent classes and utilize training samples to classify the stacked images in different dates for detecting various changes (Gao et al., 2012; Schneider, 2012). Although this kind of method is capable of achieving dynamic impervious surface maps, the ground reference data of transition types and durations for model training and validation are difficult to obtain (Volpi et al., 2013; Wu et al., 2017). By contrast, post-classification techniques classify and analyze multi-temporal images separately, which need the land cover labels in each independent image rather than conversion types, greatly reducing the difficulty and cost of acquiring samples. Although these methods have been widely used in monitoring urbanization (Bagan and Yamagata, 2012; Qin et al., 2017), they neglect the inherent relevance among the classified impervious surface maps, making additional temporal consistency techniques necessary and resulting in discontinuous achievements with a low temporal resolution (Gong et al., 2019a; Li et al., 2015; Zhang et al., 2017). Therefore, monitoring long-term dynamic impervious change will be much more difficult with time-series remote sensing images consideration. Moreover, the efficiency and accuracy of mapping dynamic impervious surfaces are still needed to be improved.

2.2. Monitoring continuous land surface phenology

LSP can currently be obtained from two main sources including site-based observation (Jochner et al., 2013; Luo et al., 2007) and phenology indicators derived from remote sensing observations (Cong et al., 2012; Piao et al., 2015). The in-situ observation stations can continue capturing high quality and long-term phenology information. However, in contrast to remote sensing-based observations that can obtain cost-effective, large-scale spatio-temporal patterns of LSP, in-situ observations are only suitable for individual small-area applications. Consequently, many studies have been conducted for exploring the LSP of various kinds of vegetation species (Pan et al., 2012; Senf et al., 2017; Zhang et al., 2003) and their changes (Cong et al., 2013; Heumann et al., 2007; Liu et al.,

2016) using different sources of time-series remotely sensed images, which provided solid foundation for further exploring the relationship between urbanization and phenology change.

2.3. Limitations of the previous works

Some approaches proposed for quantitative evaluation of phenology changes introduced by urbanization are based on the statistics and comparison of phenology indicators in the mapped urban and corresponding rural areas (Li et al., 2017; Zhou et al., 2016), which achieve convincing results and conclusions. However, some deficiencies exist in these methods and can be further improved. First, the boundaries of urban clusters in these methods are fixed during the whole study period. In fact, the urban areas have constantly expanded over time, causing inconsistency between obtained and actual urban-rural areas with fixed boundaries, which degrades the accuracy. Second, most studies achieve the results with the coarse spatial resolution more than 250 m primarily based on the nighttime light data and Moderate Resolution Image Spectroradiometer (MODIS) vegetation products, leading to some errors or even neglect of urban clusters at finer spatial scales. In addition, monitoring the difference of long-term phenology trends in urban and rural regions is a difficult task in previous studies since they have to focus on independent short-term phenology analysis with discontinuous land cover maps representing the urbanized and rural areas in different periods. Last but not least, previous methods are also hard to achieve the phenology shifts directly caused by the land cover changes of urbanization.

Therefore, the objectives of the present paper is to propose a framework based on Ensemble Continuous Change Detection and Classification (ECCDC) and Enhanced spatial and temporal adaptive reflectance fusion model (ESTARFM) for exploring comprehensive LSP impacts of urbanization, as well as for comparing the difference in LSP analysis depending on whether or not land cover change and finer spatio-temporal phenology are taken into account. Three major questions associated with phenology impacts of urbanization are considered in this study: 1) What are the phenology differences between dynamic urban and rural areas? 2) What are the differences of the phenology trends between the permanent urban and rural areas (refers to the urban and rural areas without land cover changes, hereafter)? 3) What are the phenology shifts (refers to abrupt transitions of phenology due to land cover changes, hereafter) of the urbanized regions brought by different kinds of land cover transitions?

3. Study area and data source

3.1. Study area

The study area is Nanjing City (31°14′-32°37′N, 118°22′-119°14′), China, which is located in the lower reaches of the Yangtze River and covers an area of 6587.02 km^2 with a population of 8.44 million (Fig. 1) (Nanjing Statistics Yearbook, 2018). With the warm and rainy subtropical climate and the influence of Yangtze Delta's rapid development of economic and transport background, it comes to be one of the richest agricultural areas as well as the fastest urbanized city in China. Nanjing was selected as the study area for two main reasons. First, Nanjing exemplifies many other cities in China that have been experiencing a significant urbanization process in the past decades. During 2001 to 2018, the population of Nanjing has increased by 20.65%. The economy of Nanjing has grown tremendously with the regional Gross Domestic Product increasing from $16.42 billion in 2001 (Nanjing Statistics Yearbook, 2001) to $182.98 billion in 2018 (Nanjing Statistics Yearbook, 2018). Meanwhile, rapid industrialization and infrastructure construction resulted in massive land cover changes, especially for the transition from agricultural and natural lands to urban lands, which led to the substantial expansion of impervious surfaces. Second, the composition of land cover in Nanjing is diverse and heterogeneous, which provided a good opportunity to examine the phenology effects by impervious surface expansion in different regions within the city.

3.2. Landsat data

Landsat surface reflectance data of the study area were collected from Google Earth Engine (GEE), which is a cloud-based geospatial analysis platform with huge computational capabilities (Gorelick et al., 2017). All available Landsat 5, 7 and 8 Surface Reflectance Tier 1 images were obtained from the directions of "LANDSAT/LT05/C01/T1_SR", "LANDSAT/LE07/C01/T1_SR" and "LANDSAT/LC08/C01/T1_SR" in GEE, respectively. For each Landsat image, eight bands were used for the study, including six spectral bands, one thermal band and one quality assessment band (Zhu et al. 2015, 2016). Note that the Function of Mask algorithm (Zhu and Woodcock, 2012) has been considered in the quality assessment so that the quality observations such as fill, snow/ice, cloud and cloud shadow have been identified, leaving the remaining clear observations. Landsat Collection 1 is made up of three parts: Tier 1, Tier 2 and Real-Time. The data of Tier 1 were selected because they meet the formal quality criteria so that they are suitable for time-series analysis. Due to the inherent mechanism of the ECCDC model, there may be occasional gaps in the results of the first and last years. Therefore, the total 535 Landsat images were used in this study during the period from 1999 to 01-01 to 2019-06-09, including 169 Landsat 5 images, 265 Landsat 7 images, and 101 Landsat 8 images. The images in each season from spring to winter are 138, 124, 136 and 137 respectively, which are approximately equal in each season, providing a good condition for fitting the function of seasonal components. The temporal distribution of the total Landsat reflectance observations is displayed in Fig. 2.

3.3. MODIS data

MODIS 16-Day Enhanced Vegetation Index (EVI) composite data with the 250 m spatial resolution were collected from the direction of "MODIS/006/MOD13Q1" in GEE in order to extract phenology from 2001-02-18 to 2019-06-09. At the same time, Landsat 5, 7 and 8 32-Day EVI composite data with the 30 m resolution were also collected from the directions of "LANDSAT/LT05/C01/T1_32DAY_EVI", "LANDSAT/LE07/C01/T1_32DAY_EVI" and "LANDSAT/LT05/C01/T1_32DAY_EVI" in GEE in conjunction with MODIS EVI data to enhance and match the spatial resolution of the ECCDC results. In total, 446 MODIS EVI images and 276 Landsat EVI images were obtained in this study.

3.4. Auxiliary data

In addition to Landsat and MODIS time-series images, auxiliary reference data were collected from the Geographic National Condition Census (GNCC) map of Nanjing in 2015 and very high resolution (VHR) images from Google Earth (http://earth.google.com/) in 2010 to generate the training and test samples for training and validation of ECCDC. Since the GNCC map was generated based on field visits and interpretation of aerial photographs and VHR remote sensing images, it provided land cover types of the research area with high accuracy. The classification system was defined based on Fine Resolution Observation and Monitoring of Global Land Cover (FROM-GLC) and the samples were finally extracted and categorized into 5 classes including cropland, forest, grassland, impervious surface and water in this study (Gong et al. 2013,

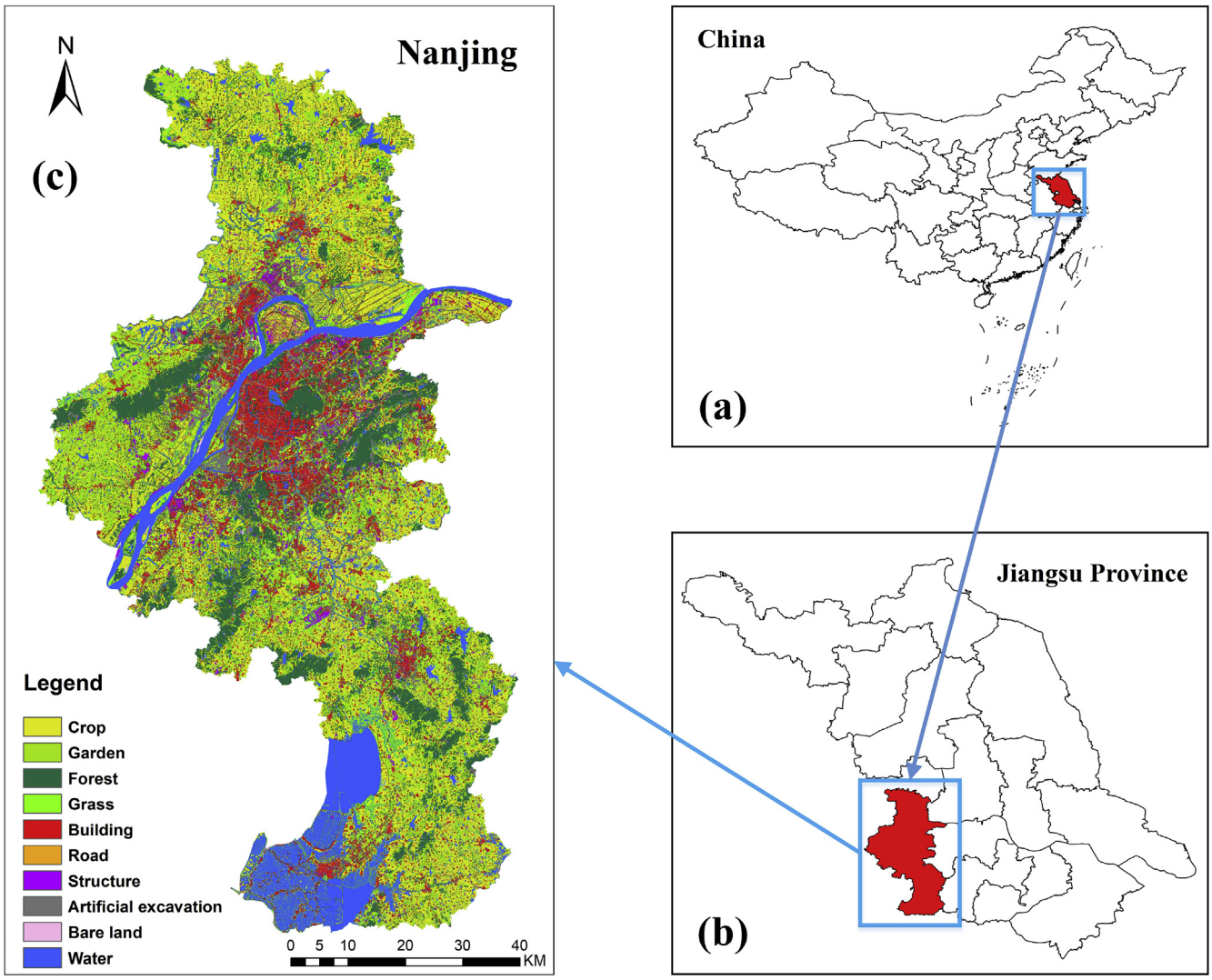

Fig. 1. Study area. (c) is the land cover map generated from Geographic National Condition Census.

2019b). The land cover types of shrub, barren and wetland in the system were excluded because their proportions were all less than 0.01% in the research area. The cloud type was also disregarded because it was removed from the process of the ECCDC algorithm as unclear observations for constructing the model.

4. Method

Fig. 3 displays the framework of the proposed approach, which is made up of three parts of works. First, dynamic urban clusters and their continuous changes were mapped based on the developed ECCDC method. Second, Landsat and MODIS times series EVI composite data were blended to achieve the high-spatiotemporal resolution EVI series for extracting phenology indicators. Finally, the phenology relationship and discrepancies between urban and rural areas were calculated through regression analysis during the period at the 30 m spatial resolution level.

4.1. Ensemble Continuous Change Detection and Classification for urban clusters

The Continuous Change Detection and Classification (CCDC) algorithm assembles all available Landsat observations for each pixel to estimate time-series models and uses the models to predict future observations (Zhu and Woodcock, 2014; Zhu et al., 2015). It has been applied to the surface reflectance (SR), brightness temperature (BT) and Normalized Differences Vegetation Index (NDVI) for land use and land cover classification and change detection. The algorithm identifies land use and land cover changes for the pixel i by using a time-series model combining seasonal and trend components (Eq. (1)).

$$\widehat{P}(i,d) = a_i + b_{1i}\cos(2\pi d/T) + b_{2i}\sin(2\pi d/T) + c_i d \quad (1)$$

where $\widehat{P}(i,d)$ is the predicted value for SR, BT or NDVI at pixel i on Julian day d. a_i and c_i are the coefficients for the trend component at pixel i, b_{1i} and b_{2i} are the coefficients for the seasonal component at pixel i, and T is 365. The model can be carried out for detecting land cover changes once 15 clear observations are available in the model initialization phase, in which 12 of them are conducted for defining the outlier of time-series model and the other 3 are used for determining whether land cover change occurs. The basis of change detection in CCDC is to compare the value of model predictions with clear observations and to normalize their difference by three times the root mean square error (*RMSE*). Once the observations of

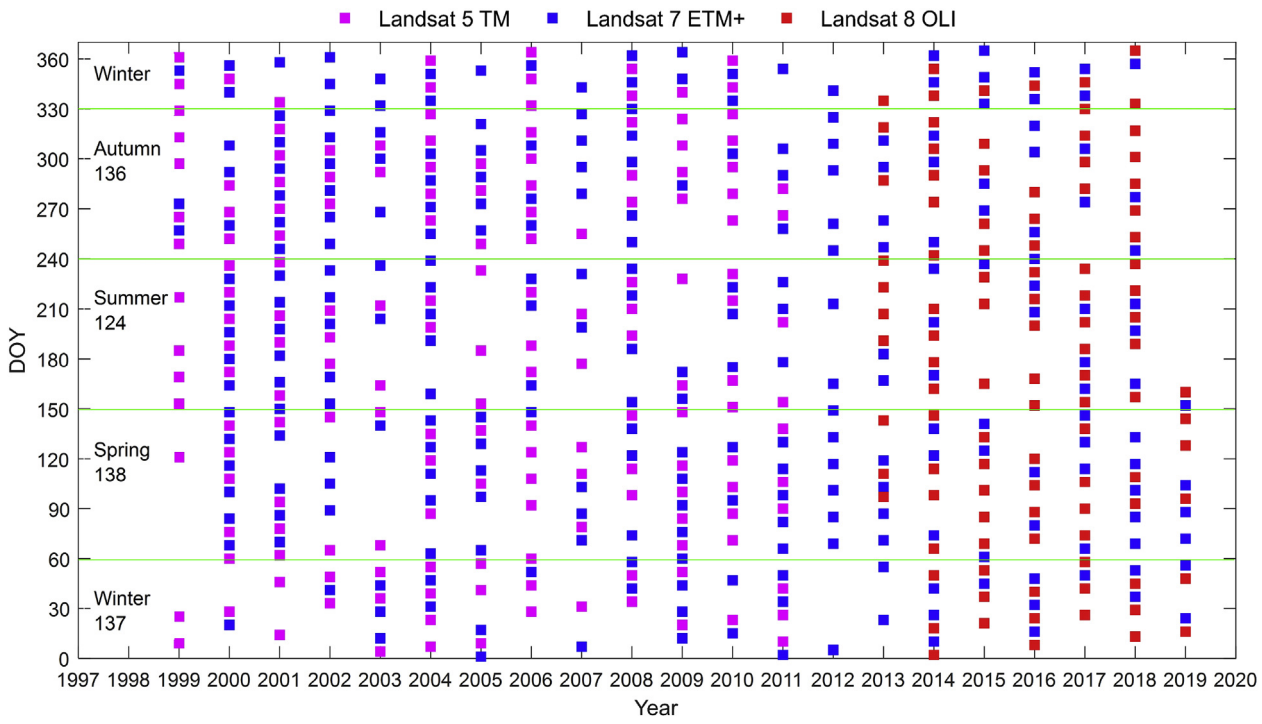

Fig. 2. Temporal distribution of Landsat 5, 7 and 8 images from 1999 to 2019.

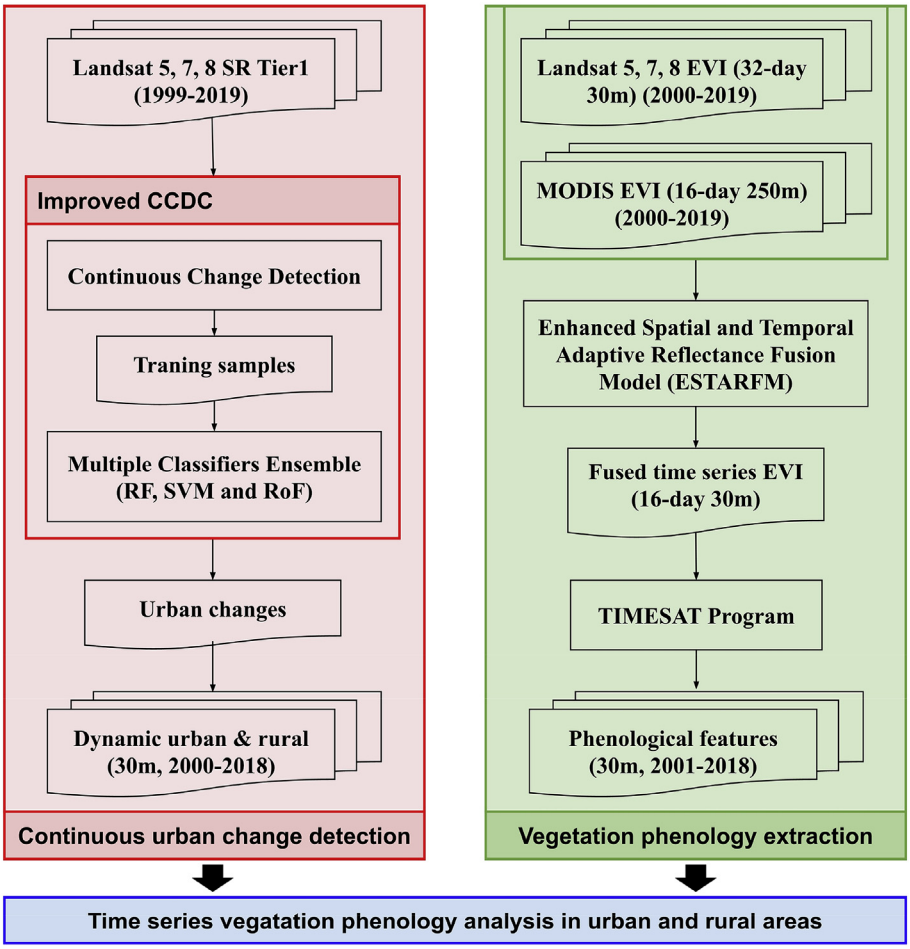

Fig. 3. The framework of the proposed approach for analyzing phenology impacts of urbanization.

three consecutive days all exceed the pre-defined threshold (Eq. (2)), the first of the three observations will be defined as the start time of land cover change.

$$\frac{1}{k}\sum_{i=1}^{k}\frac{|P(i,d)-\widehat{P}(i,d)|}{3\times RMSE_i}>1 \tag{2}$$

where k is the feature dimension of time-series data used in the algorithm. The use of three times *RMSE* considers that land cover change typically occurs when the spectral feature deviates from the prediction model by more than three times *RMSE* (Zhu and Woodcock, 2014).

After detecting changes in time-series data, land cover classification is applied to each model between breakpoints. Since different land cover types are provided with different characteristics of time-series models, the time-series classification can be conducted using a supervised classifier with the inputs of model coefficients. The original CCDC uses Random Forest (RF) as the classifier to classify the models. However, in the context of the pattern recognition field, there is no guarantee that one specific classifier can always achieve good performance in any conditions of training samples and extracted features (Chi et al., 2009). Moreover, many uncertainties still exist in the classification process considering the parameters of a time-series model rather than reflectance-based characteristics as input features (Healey et al., 2018). Thus, to enhance the reliability and robustness of the classification process, multiple classifier ensemble method is embedded in the CCDC algorithm, in which RF, Support Vector Machine (SVM) and Rotation Forest (RoF) are integrated to take advantage of multiple classifiers in this study. Then, the majority voting (MV) is carried out to identify the most frequent results of classified land cover types for each pixel during a period (Wang et al., 2018). For the case of a tie in MV, the result with the highest posterior probability will be considered as the final land cover type, as the higher posterior probability provided higher reliability for the supervised classification result (Castellana et al., 2007) (Eq. (3)). In this way, a better result for each time-series model can be defined through an enhanced way of CCDC.

$$C_{final}=\begin{cases} MV(C_1,C_2,C_3) \\ max(C_1|X,C_2|X,C_3|X) \quad if \;\; C_1\neq C_2\neq C_3 \end{cases} \tag{3}$$

where C_1 , C_2 and C_3 represent the classification results with RF, SVM and RoF classifier in ECCDC, separately. X means all the possible classification results. C_{final} represents the final classification results of each pixel in a period.

4.2. Fusion of Landsat and MODIS EVI time-series data

The vegetation indices derived from the original Landsat observations are not the best choice for extracting phenology information since they are not evenly distributed in each year. MODIS EVI composite products are sequential data provided with a stable 16-day high temporal resolution but a medium spatial resolution of 250 m, which is too coarse to match the ECCDC results with the 30 m spatial resolution. However, Landsat EVI composite products are provided with a higher spatial resolution of 30 m but a lower temporal resolution of 32 days, which is insufficient for smoothing consecutive data and extracting phenology. Therefore, it is vital to combine the advantages of the high-temporal frequency of MODIS EVI composite data and the high-spatial resolution of Landsat EVI composite data. ESTARFM (Zhu et al., 2010), which is an effective and mature fusion model for a different source of remote sensing data based on the spectral unmixing theory and "conversion coefficient" prediction method, was selected to fuse the MODIS EVI and Landsat EVI data in this research. ESTARFM is an enhanced development based on the Spatial and Temporal Adaptive Reflectance Fusion Model (STARFM) (Gao et al., 2006), which blends the high-frequency temporal information from MODIS and the high-resolution spatial information from Landsat to generate synthetic surface reflectance products at both a high temporal and spatial resolution, and can better predict the reflectance of sub-pixel consisting of heterogeneous landscapes. Like STARFM, ESTARFM predicts pixel values based on the spatially weighted difference computation between some observation pairs of Landsat EVI and MODIS EVI data, and some other MODIS EVI data at the prediction days. In this study, four pairs of cloudless MODIS and Landsat EVI composite data in close dates in all seasons of a year were used to calculate the fusion model, which can not only cover the general vegetation growth and land surface condition in each year but also accelerate the model initialization and generalization process. Then, all the MODIS EVI composite data in this year were used for predicting the corresponding fusion EVI results. These steps were repeated for each year during the period and finally, all of the 16-day EVI fusion data with the 30 m resolution from 2001 to 2018 were generated.

4.3. Extraction of phenology metrics

The adaptive Savitzky-Golay method embedded in TIMESAT 3.3 was conducted for smoothing the time-series EVI fusion data (Jönsson and Eklundh, 2004), as it had good performances on dealing with continuous vegetation indices (Chen et al., 2004; Heumann et al., 2007). In this research, we focused on three indicators to explore the phenology relationship between urban and rural areas, including SOS, EOS, and GSL. The SOS and EOS are defined when the fitted curve reaches a proportion of the seasonal amplitude measured from the left and right minimum values respectively (Shen et al., 2015; Zhou et al., 2016). According to the previous experiences, the threshold of seasonal amplitude proportion was defined as 20% from the left and right minimum levels (Brown et al., 2010; Buyantuyev and Wu, 2012; Cong et al., 2012; White et al., 2009; Zhou et al., 2016). The GSL was defined as the length of the dates between SOS and EOS. Fig. 4 shows an example of the Savitzky-Golay smoothing and phenology extraction in a pixel of the study area during a period.

The SOS, EOS, and GSL were separately calculated for each year during the period from 2001 to 2018. Due to the complexity of the surface land in urban areas, the outliers of the phenology indicators were set up with the combination of the previous experiences and practices: 1) pixels with SOS earlier than the 30th day or later than the 180th day of a year were excluded for analysis; 2) EOS of each pixel was constrained between the 240th and 360th day of a year (Cong et al., 2012; Li et al., 2017; Zhang et al., 2006). Following the general practices in previous studies, we did not attempt to make a validation for the generated phenology information by field observations owing to the different definitions in ecosystem and species and various uncertainty sources (Rodriguez-Galiano et al., 2015).

4.4. Analysis of phenology impact of urbanization

For accurately exploring the phenology response to urbanization in Nanjing, continuous change detection and classification of urban clusters are taken into account. For rural areas, different from directly using a buffer extending from the urban center with a fixed radius, the extents were delineated by keeping their sizes to be the same as the corresponding urban areas each year. It can be mapped by slightly increasing the radius of rural extents based on the initial

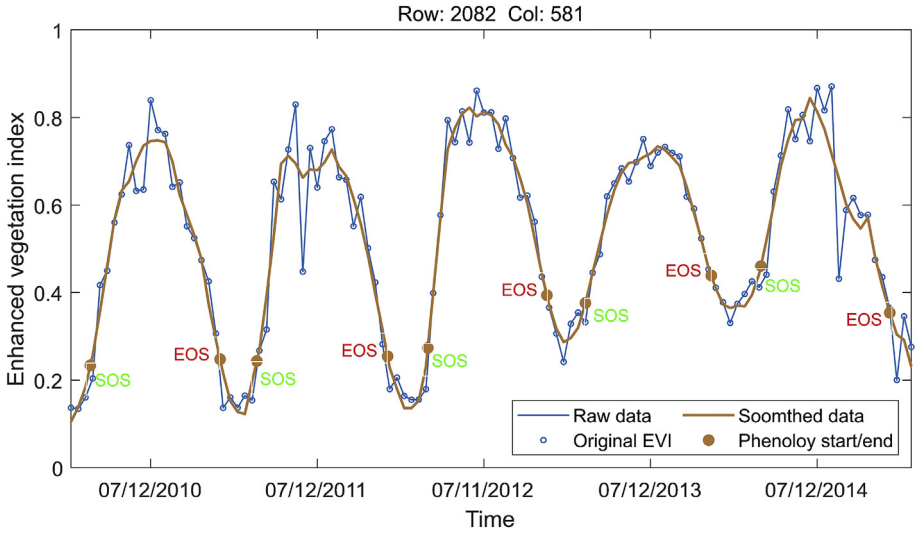

Fig. 4. An example of the smoothing process based on Savitzky-Golay method and phenology extraction from time-series vegetation indices.

shape of the classified urban clusters until their area equal to the corresponding urban areas (Li et al., 2017). This method can assure the rural areas are provided with the same sizes as the associated urban region. In addition, the urban clusters smaller than 10 × 10 pixels were excluded since they were not provided with independent and stable LSP. The pixels in the rural areas with the land cover type of water were also excluded due to the low vegetation coverage in the water body. Thus, dynamic annual urban-rural clusters are defined in Nanjing from 2001 to 2018.

4.4.1. Analysis of phenology difference between urban and rural areas

To explore the phenology difference between urban and rural areas in the whole period, the average phenology of each urban and the corresponding rural cluster in each year were calculated, and simple linear regression based on weighted least squares (WLS) estimate was conducted (Eq. (4)).

$$S = min(\sum_{i=1}^{n} W_i(y_i - aX_i)^2) \quad (4)$$

where y_i represents the ith actual value. a is the slope of the fitted simple linear function and aX_i means the ith estimated value. W_i represents the ith weight which is used by the area of urban cluster in this study. S represents the weighted sum of squares and a achieves the optimal solution when S reaches the minimum value. The direction of phenology impacts can be obtained by comparing the slope a with 1. The significance test of the regression model was also carried out, and phenology difference was significant when p was lower than 0.01.

4.4.2. Analysis of the difference of phenology trend between urban and rural areas

Under the background of global climate change, LSP is also provided with a long-term changing trend (Richardson et al., 2013). Due to the discrepancies in the urban and rural local environments, it is necessary to explore the performance of phenology trends in different regions. However, land cover changes will disturb the original phenology trends under climate conditions. To address this problem, the pixels with land cover changes were excluded based on ECCDC. Furthermore, unique labels for each urban and rural pixel in each year were made, and the pixel labels which are same throughout the period were reserved as the permanent urban-rural cluster pairs. Ordinary Least Squares (OLS) regression was applied on the phenology of all years for each permanent urban and rural pixel to describe their changing trends. At last, simple linear regression based on WLS estimate and its significance test were conducted to achieve the overall discrepancies of their phenology trends.

4.4.3. Analysis of phenology shift due to the land cover change

Since ECCDC can achieve the changing time and type of impervious surface change, it provides a good opportunity to analyze the phenology shift by land cover changes and to categorize them by changing type, which is of great significance to understand the direct phenology impacts of urbanization. For this purpose, the changing time in each pixel was used as a cut-off point. The average phenology indicators before and after the changing time were calculated and compared in each pixel changed to the impervious surface during the time.

5. Results

5.1. Continuous change detection and classification of urban land

Based on all available Landsat 5, 7 and 8 images, training samples and ECCDC algorithm, the change detection and classification results of each pixel in the study area during the period from 2000 to 2018 were achieved. Eventually, 19 annual land cover maps were also compiled and available in Appendix A (Fig. A) based on the extraction of ECCDC model on the middle day of each year. Since we only focused on the urbanization process during this period, the changing location and time of the pixels in which all the other land cover types transformed to the impervious surface were extracted and recorded (Fig. 5). The urban areas have expanded much with 736.50 km^2 (11.18% of the total area) urbanized in the past 19 years. The cropland and some other natural lands such as forest, grassland, and water have been shrinking and replaced by impervious surfaces. In terms of the location, the main urban expansions in Nanjing happened based on the original urban clusters, which were the cores of downtown areas located along the south and north banks of the Yangtze River. The closer to the core urban clusters, the earlier occurred impervious surface expansion, which was consistent with the changing time results displayed in Fig. 5(a). From the

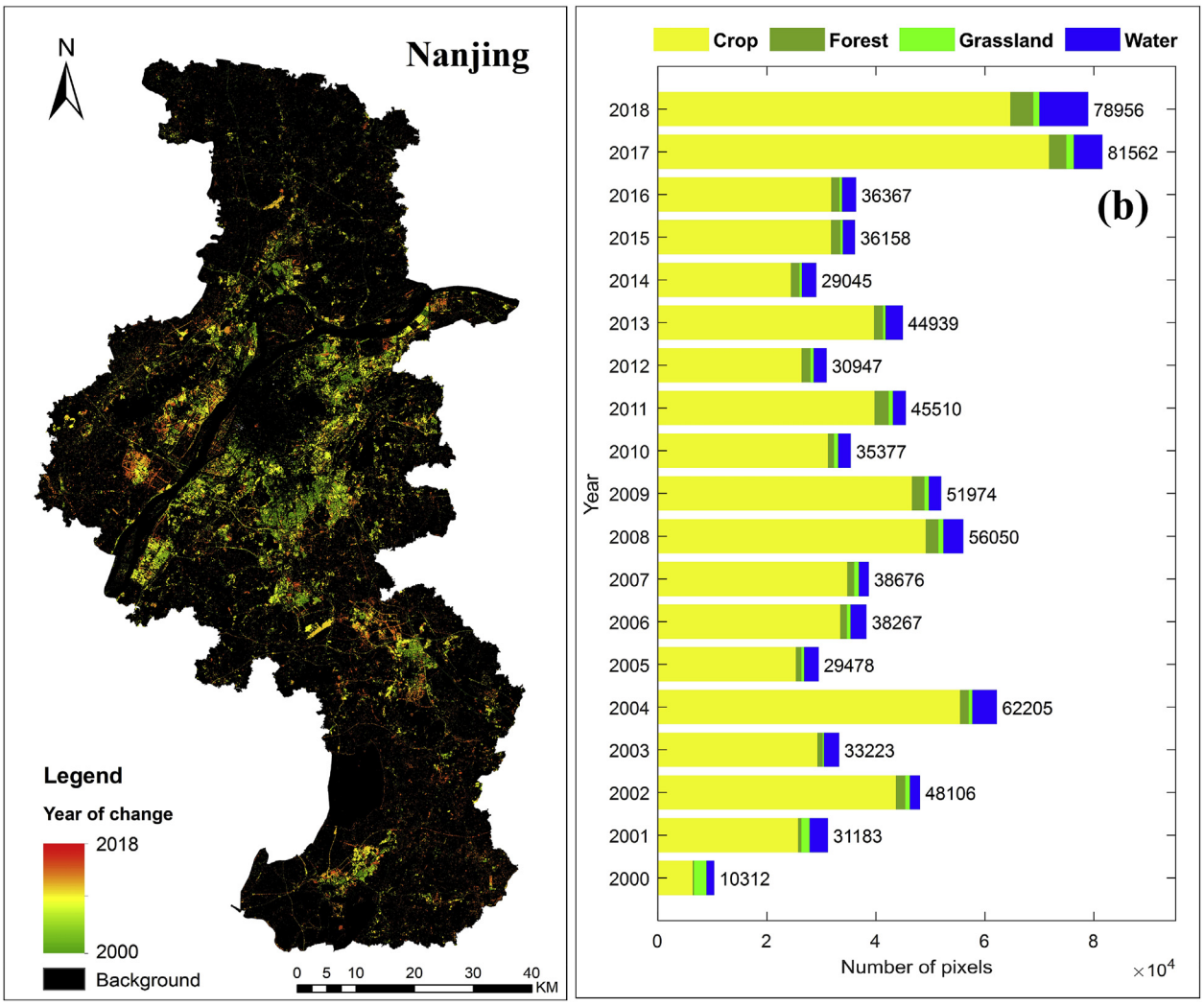

Fig. 5. Change detection of impervious surfaces in Nanjing from 2000 to 2018. (a) Changing location and time of impervious surface areas and (b) statistics of the land covers converted to impervious surfaces.

aspect of conversion type, 86.80% of these areas were cropland before urbanization since it was the dominant land cover type in Nanjing and distributed surrounding the urban clusters, followed by water (7.23%), forest (4.00%) and grassland (1.97%) (Fig. 5(b)).

The classification results were assessed by randomly splitting the selected 10,000 samples into two groups including 5000 training samples and the other 5000 test samples in 2015 based on the summary and interpretation of GNCC, FROM-GLC and Google Earth history maps for training the time-series model and cross-validation, respectively. For the case of evaluating change detection results, the pixels in 2010 with the same location of the test samples in 2015 were interpreted and labeled based on the FROM-GLC and Google Earth historical map in 2010 (Fu and Weng, 2016). After excluding some uncertain samples during the interpretation process, 4818 training samples in 2015 for training ECCDC model, 4342 test samples in 2015 for validation of the classification results and 2804 sample pairs between 2010 and 2015 for change detection evaluation were finally obtained, respectively. Table 1 shows the classification results, in which the overall accuracy reached 96.71% with a Kappa coefficient of 95.22%. The worst type of classification result was grassland with user's and producer's accuracy of 80.20% and 86.17% owing to its low coverage and easily-confused reflectance features with cropland. The user's and producer's accuracy of the impervious surface were 95.91% and 95.56%, which proved the effectiveness and reliability of the method for

Table 1
Error matrix of accuracy assessment of classification results.

	Cropland	Forest	Grassland	ISA	Water	UA
Cropland	1967	10	2	27	12	97.47%
Forest	11	446	1	2	0	96.96%
Grassland	9	0	81	3	8	80.20%
ISA	27	3	3	797	1	95.91%
Water	10	2	7	5	908	97.42%
PA	97.18%	96.75%	86.17%	95.56%	97.74%	96.71%

Note: ISA, UA and PA represent the impervious surface area, user's accuracy, and producer's accuracy, respectively.

Table 2
Accuracy of change detection results.

	Non-change	Change	User's accuracy
Non-change	2784	2	99.93%
Change	2	16	88.89%
Producer's accuracy	99.93%	88.89%	99.86%

monitoring the urbanization in Nanjing. For the change detection results, the user's and producer's accuracy of change and no-change were both 88.89% and 99.93%, providing quality assurance for monitoring change occurrence (Table 2).

Once the consecutive urban clusters in each term are recognized by the results of ECCDC, the corresponding successive rural areas can be sequentially figured out and mapped through the buffer method mentioned before (Fig. 6). It can be seen from the figures that both urban and rural areas have greatly expanded during the study period, which proves the necessity of using accurate continuous dynamic urban-rural boundaries to explore the urbanization implications for LSP at a city scale.

5.2. Land surface phenology with a fine spatio-temporal resolution

Based on the time-series fusion images from the ESTARFM model, fine spatio-temporal time-series EVI data were generated. To validate the effectiveness of the fusion images, phenology indicators of all the urban-rural areas in all years were extracted from both MODIS and fusion EVI images. As the spatial resolution of original MODIS data is far coarser than the land cover maps of ECCDC results, the phenology of the pixels close to the boundaries of urban-rural areas will be homogenized and given the same values, resulting in a reduction in phenology difference between urban and rural regions. The longer the boundary line and the smaller the size of urban clusters, the larger the error will be. Therefore, the results based on fusion EVI-based phenology can better reflect the respective phenology information at the location than the original MODIS data. The phenology difference between urban-rural clusters and the comparison of urban-rural phenology difference between MODIS and fusion EVI were conducted by Eq. (5) and (6), respectively.

$$\Delta P = P_{ub} - P_r \tag{5}$$

$$D = \Delta P_{Fusion} - \Delta P_{Modis} \tag{6}$$

where ΔP is the difference of three indicators (i.e., SOS, EOS and GSL) between urban (P_{ub}) and the corresponding rural clusters (P_r). D is the difference of three urban-rural phenology indicator

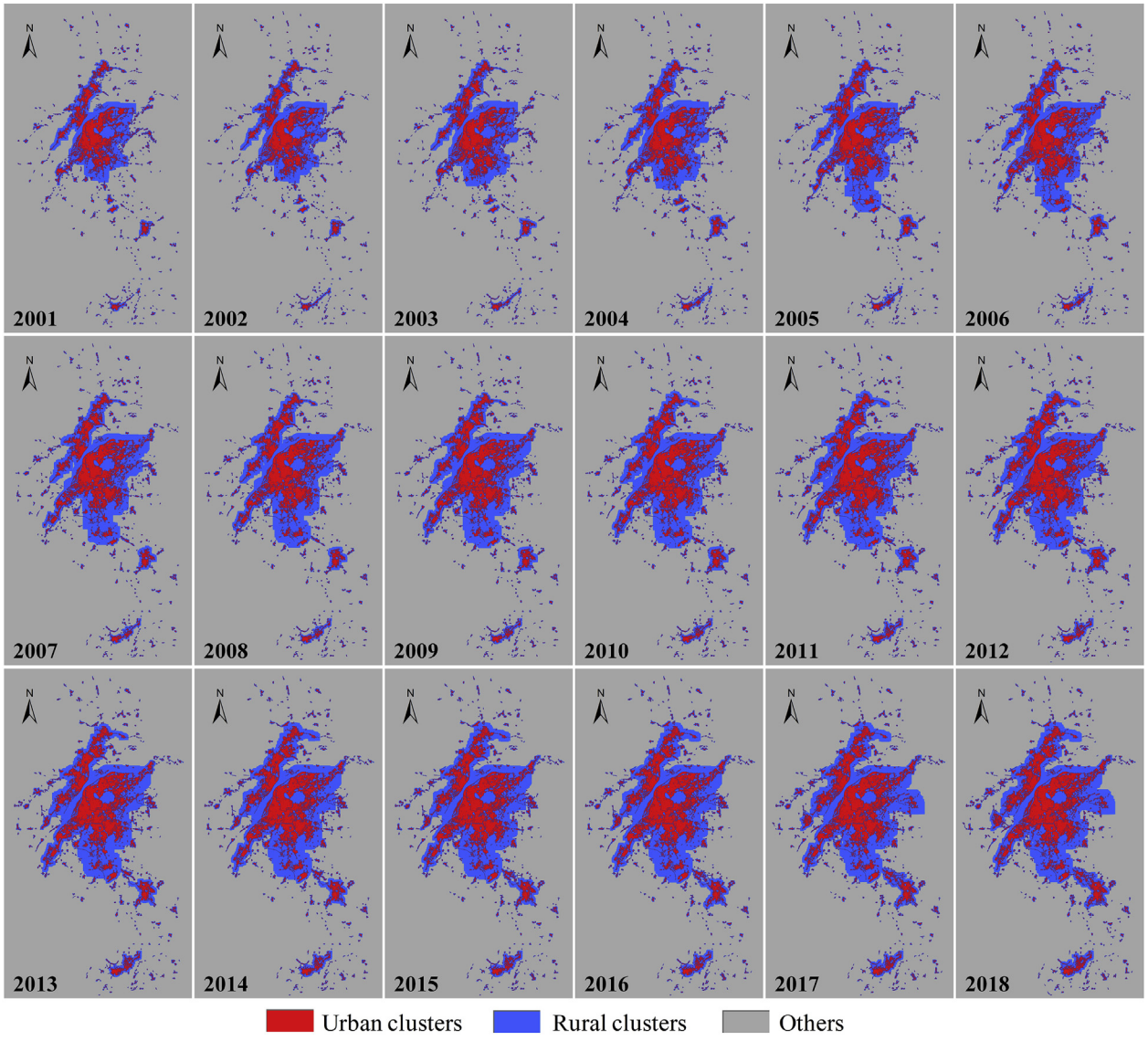

Fig. 6. Urban-rural land cover maps under the process of urbanization in Nanjing from 2001 to 2018.

differences between fusion (ΔP_{Fusion}) and MODIS (ΔP_{Modis}) time-series EVI. Therefore, a positive ΔP for EOS/GSL or a negative ΔP for SOS indicates a prolonging impact on vegetation growing length and vice versa. A positive D for EOS/GSL or a negative D for SOS demonstrates the impact of eliminating the error at urban-rural boundaries and vice versa. Fig. 7 descries the D of all urban-rural clusters in Nanjing. The average D of SOS was negative and the percentage is more than 50%, and the conditions were opposite in EOS and GSL. That is to say, using fusion EVI data enlarged the SOS advance, EOS delay and GSL prolonging of urban clusters compared with MODIS EVI data, which proofed the effectiveness of fusion EVI data in reducing the phenology errors at urban-rural boundaries.

5.3. Phenology difference between urban and rural areas

The three phenology indicators including SOS, EOS and GSL displayed significant differences in urban and rural areas in Nanjing from 2001 to 2018. Fig. 8 shows the scatters represented the three phenology indicators in the urban and rural areas of all years during the whole period. Overall, the phenology in urban and rural areas under the control of similar climate background appeared to be highly correlated, as indicated in the regression lines of the scatters closed to $y = x$ with all $R^2 > 0.91$ and $p < 0.01$. The SOS occurred 0.59 ± 0.58 days earlier in urban areas than that in rural areas as suggested by the slope of <1 (i.e., 0.991). While, the slope of EOS was 1.005, manifesting EOS 1.65 ± 1.55 days later in urban regions. As a result, the GSL was 2.77 ± 2.61 days extended in urban areas with a slope of 1.011. Vegetation can grow only if the temperature reaches a certain threshold and it has been proven that they were provided with a significant positive correlation in many typical cases (Shen et al., 2011; Wang et al., 2015). Therefore, the results in our research were mainly attributed to the higher temperature in urban areas caused by UHI effect (Imhoff et al., 2010; Zhou et al., 2016), providing powerful evidence that the urban environment had implications on LSP and continues with the urbanization process.

5.4. Difference of phenology trend in urban and rural areas

Since the permanent urban-rural areas in Nanjing were determined based on ECCDC and label matching, the spatial pattern of the regions was mapped in Fig. 9(a). It can be seen from the figure that the scope of the permanent urban-rural regions was much smaller than their annual distributions, which also indicated that the urban clusters expanded significantly during the period. After applying OLS regression on the phenology during the whole period, phenology trends in each permanent urban and rural pixel were achieved. Apparent discrepant trends of SOS, EOS, and GSL in different regions can be discovered from Fig. 9(b)–(d).

Fig. 10 shows the scatter patterns of average phenology trends in each permanent urban and rural clusters. WLS estimate was also applied to the scatters for regression in each plot (Eq. (6)). Two conclusions can be drawn from the plots: 1) 70.81%, 78.79% and 80.72% of scatters in the plot of SOS, EOS and GSL trends fell in the first quadrant of the coordinate axis, which means that SOS and EOS were provided with the delay trend and GSL had an extended trend in most permanent urban and rural areas. The results demonstrated that, in the context of global climate change, LSP in both urban and rural areas has changed with the direction of increasing vegetation growing cycles. 2) The slopes of the regression lines in SOS and EOS were both <1, while the slope of GSL regression line was >1, which illustrated that the rates of SOS and EOS trends in rural areas were 0.12 ± 0.12 day/year and 0.02 ± 0.02 day/year faster than those in urban areas. Accordingly, the rate of GSL trend was 0.04 ± 0.04 day/year faster in urban regions compared with rural regions. These results indicated that the response of LSP in urban areas to climate change was less sensitive than that in rural areas, which was consistent with the view of urban local climate zone (Stewart and Oke, 2012). Emissions of anthropogenic activity and land surface characteristics altered local climate through modification of the composition of the atmosphere and land surface processes that influenced surface energy balance and boundary layers, leading to a distinct and insusceptible urban local climate different from global climate change (Middel et al., 2014).

5.5. Phenology shift due to land cover change

The phenology shift of each urbanized pixel was figured out based on changing time obtained from ECCDC. Fig. 11(a)-(c) mapped phenology differences before and after land cover changes. Overall, 65.77% SOS and 70.33% EOS of the changed pixels delayed

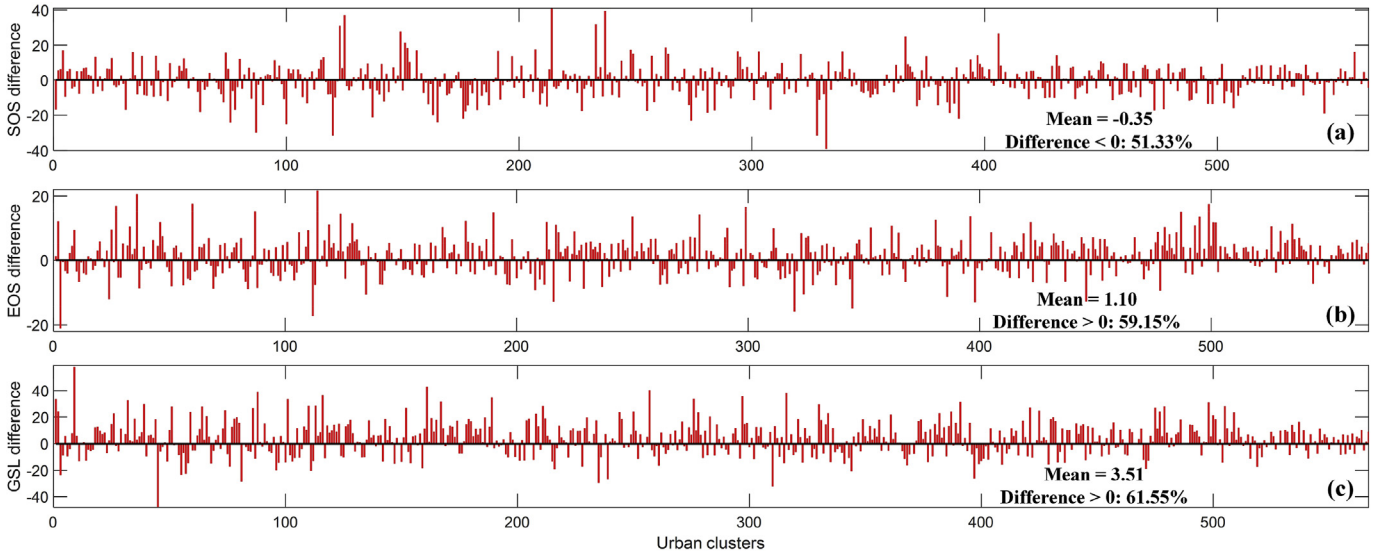

Fig. 7. Comparisons of urban-rural phenology difference between fusion EVI and MODIS EVI images. (a) SOS comparison, (b) EOS comparison and (c) GSL comparison.

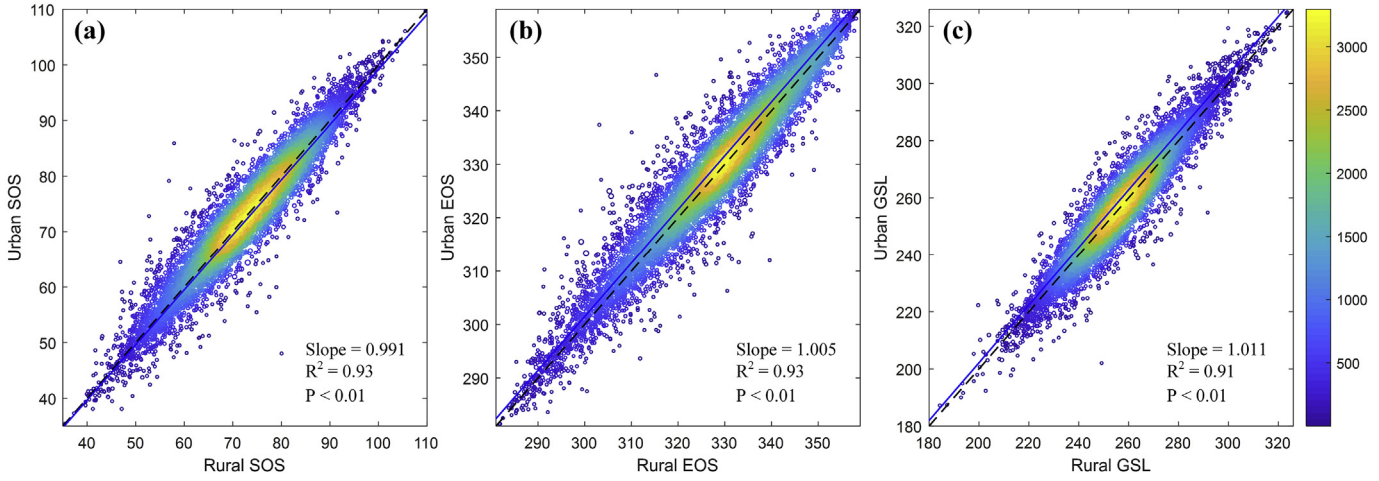

Fig. 8. Scatter points of (a) SOS, (b) EOS and (c) GSL between urban and rural areas.

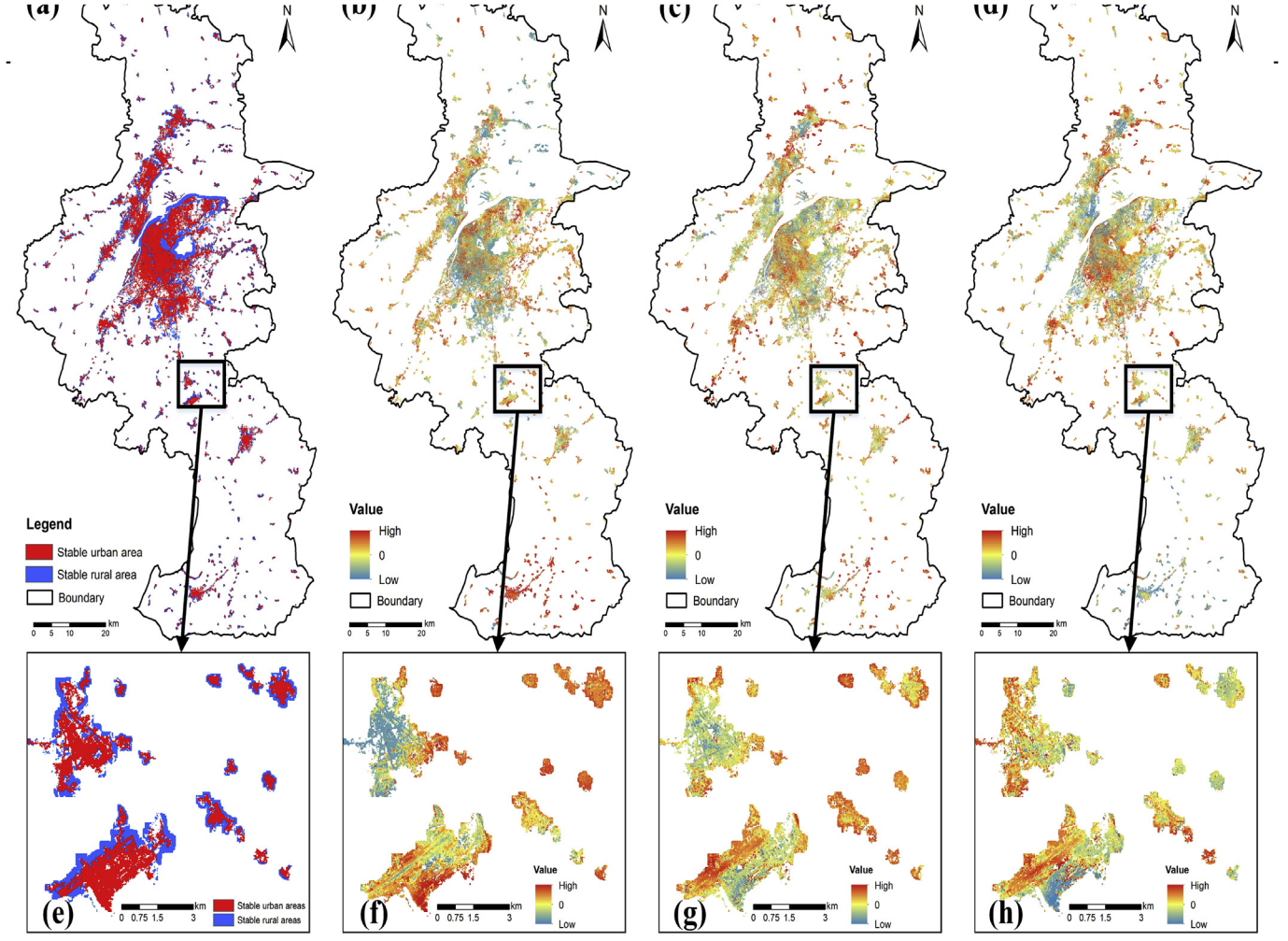

Fig. 9. (a) Permanent urban-rural cluster pairs during the study period. (b)–(d) are SOS, EOS and GSL trends in the permanent urban-rural pixels. (e)–(h) are the enlarged examples of the same regions in (a)–(d).

and 70.83% GSL of the changed pixels prolonged after transitions. For detailed exploration, the phenology shifts were grouped by changing type. As the phenology of water is close to 0, the changing type of water to the impervious surface was excluded from the analysis. Fig. 11(d)–(f) show the phenology shifts of urbanized areas categorized by land cover change type. The SOS advanced with a median value of 0.98 days for the conversion from forest to impervious, whereas the SOS postponed with median values of

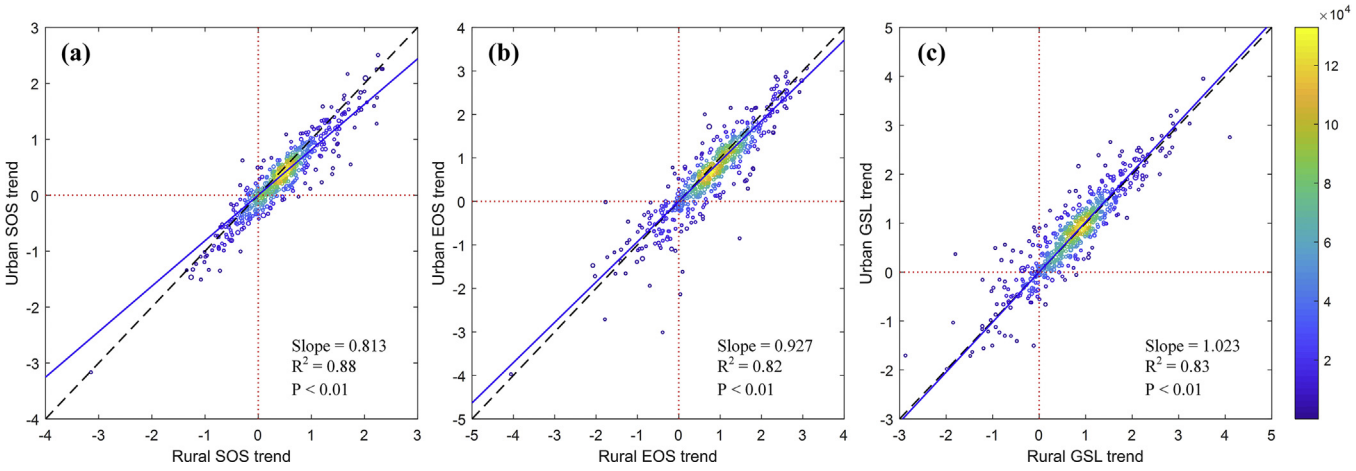

Fig. 10. Scatter patterns of (a) SOS trends, (b) EOS trends and (c) GSL trends in permanent urban-rural areas.

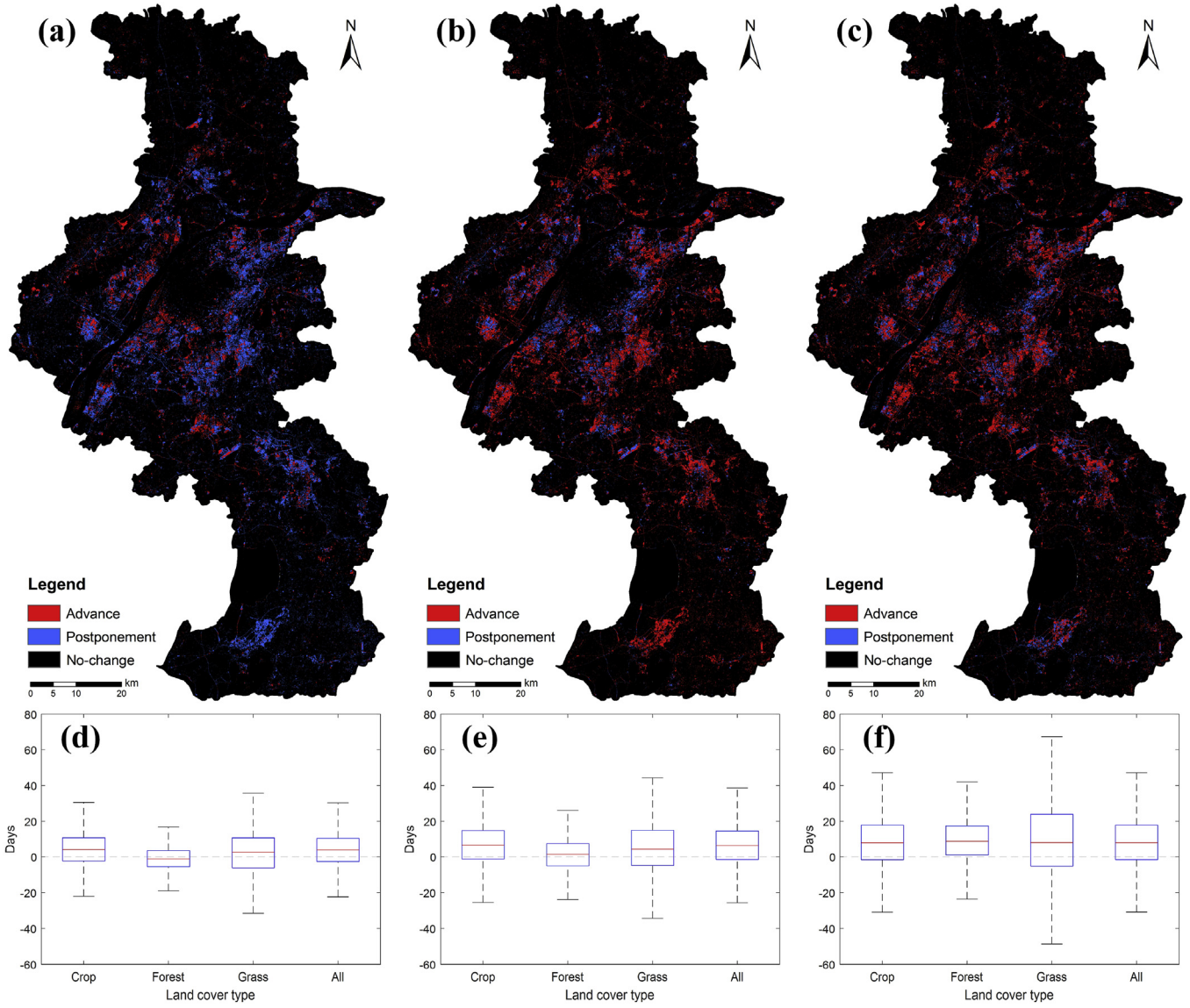

Fig. 11. (a)–(c) show the spatial patterns of phenology shifts with SOS, EOS and GSL before and after changing to impervious surfaces. (d)–(f) count the phenology shifts of SOS, EOS and GSL by conversion type.

Table 3
Comparisons of the previous approach (Pre) and the proposed approach (Pro).

	Phen-SOS		Phen-EOS		Phen-GSL		Tren-SOS		Tren-EOS		Tren-GSL	
index	Pre	Pro	Pre	Pro	Pre	Pro	Pre	Pro	Pre	Pro	Pre	Pro
slope	1.003	0.991	1.002	1.005	1.005	1.011	0.801	0.813	0.796	0.927	1.008	1.023
R^2	0.86	0.93	0.86	0.93	0.77	0.91	0.86	0.88	0.54	0.82	0.71	0.83
P	<0.01	<0.01	<0.01	<0.01	<0.01	<0.01	<0.01	<0.01	<0.01	<0.01	<0.01	<0.01

Note that Phen-SOS, Phen-EOS and Phen-GSL represent the experiments in 5.3 for SOS, EOS and GSL. Tren-SOS, Tren-EOS and Tren-GSL mean the experiments in 5.4 for SOS, EOS and GSL.

4.38 and 2.57 days for the conversions from cropland and grassland to the impervious surface. The EOS postponed with median values of 6.94, 0.63 and 5.27 days and GSL prolonged with median values of 8.40, 9.92 and 10.79 days for the conversions from cropland, forest, and grassland to the impervious surface, respectively, indicating longer vegetation growing cycles owing to the urban expansion process.

6. Discussion

The approach using fixed land cover maps and coarse-spatial-resolution time-series vegetation indices has been proven to be effective in analysis of urbanization impact on LSP in large areas (e.g., regional and global scale). However, its applicability has not been verified within the city scale. To comprehensively compare it with the proposed approach, the experiments of analyzing the difference of phenology and their trends between urbanized and rural regions (5.3 and 5.4) were also conducted with the previous method. The results of these two methods are listed in Table 3. For the phenology difference, the proposed approach was provided with larger R^2 which elucidated that it reflects the phenology differences in urbanized and rural areas more reliably. At the same time, the proposed approach also achieved results with larger R^2 in analyzing phenology trends. In contrast, for the results of these two experiments with previous method, their R^2 are smaller compared with the proposed approach, as well as their slopes are more closed to 1. Hence, the approach proposed in this work showed better performances and applicabilities on studying the response of LSP to urbanization within city scale than the previous method.

7. Conclusions

This study examined continuous urban expansion from 2000 to 2018 with sequential Landsat images and assessed its influences on LSP from a fine spatio-temporal scale. In comparison with the previous studies, this research contributed to the analysis of the LSP discrepancies between urban and rural areas with accurate dynamic urban-rural boundaries generated by ECCDC. Moreover, for exactly matching urban clusters and their changes, vegetation indices reconstruction and phenology extraction were carried out through the fusion of time-series MODIS and Landsat EVI composite images, reducing the homogenizing impact of phenology at urban-rural boundaries caused by coarse-resolution data. Taking Nanjing as a case study, the key achievements using the proposed approach were summarized as follows: 1) ECCDC method was developed and used for mapping urbanization in Nanjing from 2001 to 2018, in which urban areas expanded about 11.18% of the total area; 2) the SOS was 0.59 ± 0.58 days earlier in urban areas than that in rural areas, while the EOS was 1.65 ± 1.55 days later in urban areas, accompanied by 2.77 ± 2.61 days prolonged GSL for urban LSP; 3) the rates of SOS and EOS delay in rural areas were 0.12 ± 0.12 day/year and 0.02 ± 0.02 day/year faster than those in urban areas, along with GSL prolonging rate in urban regions 0.04 ± 0.04 day/year faster than that in rural regions; and 4) the phenology shifts of urbanized areas were provided with postponing SOS and EOS and prolonging GSL overall. However, the directions and degrees of phenology shift were diverse for different transition types in detail.

In summary, this research proposed a novel approach of LSP impacts of urbanization taking continuous land cover change and fine spatio-temporal sequential data into account. The experimental results of the typical case study in Nanjing improved the knowledge of phenology change under the influence of urbanization from different perspectives, gaining more public concerns about the relationships between urbanization and ecosystem. Futhermore, some other natural driving mechanisms and factors on LSP impacts of urbanization need to be further studied and considered in our future work.

CRediT authorship contribution statement

Xin Wang: Conceptualization, Methodology, Software, Formal analysis, Writing - original draft. **Peijun Du:** Resources, Writing - review & editing, Project administration, Funding acquisition. **Dongmei Chen:** Resources, Writing - review & editing, Supervision. **Cong Lin:** Validation, Visualization. **Hongrui Zheng:** Validation, Visualization. **Shanchuan Guo:** Data curation.

Declaration of competing interest

The authors declare that they have no known competing financial interests or personal relationships that could have appeared to influence the work reported in this paper.

Acknowledgments

The authors are grateful to the Global Environment Remote Sensing (GERS) Laboratory at the University of Connecticut for providing the algorithm code of Continuous Change Detection and Classification and to High-performance Spatial Computational Intelligence Lab (HPSCIL) at China University of Geosciences (Wuhan) for providing GPU-based Enhanced Spatial and Temporal Adaptive Reflectance Fusion Model codes. This research was supported by the National Natural Science Foundation of China (No. 41631176), China, and the Natural Sciences and Engineering Research Council of Canada (NSERC), Canada. The authors would like to thank Shahab Jozdani for his comments and suggestions to improve this manuscript. The first author would like to express his gratitude to the China Scholarship Council for supporting his stay at Queen's University, Kingston, ON, Canada.

Appendix A. Supplementary data

Supplementary data to this article can be found online at https://doi.org/10.1016/j.jclepro.2020.122487.

References

Rodriguez-Galiano, V., Dash, J., Atkinson, P.M., 2015. Intercomparison of satellite sensor land surface phenology and ground phenology in Europe. Geophys. Res. Lett. 42, 2253–2260.

Arnold Jr., C.L., Gibbons, C.J., 1996. Impervious surface coverage: the emergence of a key environmental indicator. J. Am. Plann. Assoc. 62, 243–258.

Bagan, H., Yamagata, Y., 2012. Landsat analysis of urban growth: how Tokyo became the world's largest megacity during the last 40 years. Remote Sens. Environ. 127, 210–222.

Ban, Y., Gong, P., Chandra, G., 2015. Global land cover mapping using Earth observation satellite data: recent progresses and challenges. ISPRS J. Photogrammetry Remote Sens. 103, 1–6.

Brown, M.E., de Beurs, K., Vrieling, A., 2010. The response of African land surface phenology to large scale climate oscillations. Remote Sens. Environ. 114, 2286–2296.

Buyantuyev, A., Wu, J., 2012. Urbanization diversifies land surface phenology in arid environments: interactions among vegetation, climatic variation, and land use pattern in the Phoenix metropolitan region, USA. Landsc. Urban Plann. 105, 149–159.

Castellana, L., D'Addabbo, A., Pasquariello, G., 2007. A composed supervised/unsupervised approach to improve change detection from remote sensing. Pattern Recogn. Lett. 28, 405–413.

Cecchi, L., d'Amato, G., Ayres, J., Galan, C., Forastiere, F., Forsberg, B., Gerritsen, J., Nunes, C., Behrendt, H., Akdis, C., 2010. Projections of the effects of climate change on allergic asthma: the contribution of aerobiology. Allergy 65, 1073–1081.

Chen, J., Jönsson, P., Tamura, M., Gu, Z., Matsushita, B., Eklundh, L., 2004. A simple method for reconstructing a high-quality NDVI time-series data set based on the Savitzky–Golay filter. Remote Sens. Environ. 91, 332–344.

Chi, M., Kun, Q., Benediktsson, J.A., Feng, R., 2009. Ensemble classification algorithm for hyperspectral remote sensing data. Geosci. Rem. Sens. Lett. IEEE 6, 762–766.

Clinton, N., Gong, P., 2013. MODIS detected surface urban heat islands and sinks: global locations and controls. Remote Sens. Environ. 134, 294–304.

Cong, N., Piao, S., Chen, A., Wang, X., Lin, X., Chen, S., Han, S., Zhou, G., Zhang, X., 2012. Spring vegetation green-up date in China inferred from SPOT NDVI data: a multiple model analysis. Agric. For. Meteorol. 165, 104–113.

Cong, N., Wang, T., Nan, H., Ma, Y., Wang, X., Myneni, R.B., Piao, S., 2013. Changes in satellite-derived spring vegetation green-up date and its linkage to climate in China from 1982 to 2010: a multimethod analysis. Global Change Biol. 19, 881–891.

Du, J., Qian, L., Rui, H., Zuo, T., Zheng, D., Xu, Y., Xu, C.-Y., 2012. Assessing the effects of urbanization on annual runoff and flood events using an integrated hydrological modeling system for Qinhuai River basin, China. J. Hydrol. 464, 127–139.

Feyisa, G.L., Meilby, H., Jenerette, G.D., Pauliet, S., 2016. Locally optimized separability enhancement indices for urban land cover mapping: exploring thermal environmental consequences of rapid urbanization in Addis Ababa, Ethiopia. Remote Sens. Environ. 175, 14–31.

Fu, P., Weng, Q., 2016. A time series analysis of urbanization induced land use and land cover change and its impact on land surface temperature with Landsat imagery. Remote Sens. Environ. 175, 205–214.

Gaku, K., Nishikawa, Y., Kasagi, T., Kosuge, S., 2004. Does seed production of spring ephemerals decrease when spring comes early? Ecol. Res. 19, 255–259.

Gao, F., Masek, J., Schwaller, M., Hall, F., 2006. On the blending of the Landsat and MODIS surface reflectance: predicting daily Landsat surface reflectance. IEEE Trans. Geosci. Rem. Sens. 44, 2207–2218.

Gao, F., de Colstoun, E.B., Ma, R., Weng, Q., Masek, J.G., Chen, J., Pan, Y., Song, C., 2012. Mapping impervious surface expansion using medium-resolution satellite image time series: a case study in the Yangtze River Delta, China. Int. J. Rem. Sens. 33, 7609–7628.

Gazal, R., White, M.A., Gillies, R., Rodemaker, E.L.I., Sparrow, E., Gordon, L., 2008. GLOBE students, teachers, and scientists demonstrate variable differences between urban and rural leaf phenology. Global Change Biol. 14 (7), 1568–1580.

Gong, P., Wang, J., Yu, L., Zhao, Y., Zhao, Y., Liang, L., Niu, Z., Huang, X., Fu, H., Liu, S., 2013. Finer resolution observation and monitoring of global land cover: first mapping results with Landsat TM and ETM+ data. Int. J. Rem. Sens. 34, 2607–2654.

Gong, P., Li, X., Zhang, W., 2019a. 40-Year (1978–2017) human settlement changes in China reflected by impervious surfaces from satellite remote sensing. Sci. Bull. 64, 756–763.

Gong, P., Liu, H., Zhang, M., Li, C., Wang, J., Huang, H., Clinton, N., Ji, L., Li, W., Bai, Y., 2019b. Stable classification with limited sample: transferring a 30-m resolution sample set collected in 2015 to mapping 10-m resolution global land cover in 2017. Sci. Bull. 64, 370–373.

Gorelick, N., Hancher, M., Dixon, M., Ilyushchenko, S., Thau, D., Moore, R., 2017. Google Earth engine: planetary-scale geospatial analysis for everyone. Remote Sens. Environ. 202, 18–27.

Healey, S.P., Cohen, W.B., Yang, Z., Brewer, C.K., Brooks, E.B., Gorelick, N., Hernandez, A.J., Huang, C., Hughes, M.J., Kennedy, R.E., 2018. Mapping forest change using stacked generalization: an ensemble approach. Remote Sens. Environ. 204, 717–728.

Heumann, B.W., Seaquist, J., Eklundh, L., Jönsson, P., 2007. AVHRR derived phenological change in the Sahel and Soudan, Africa, 1982–2005. Remote Sens. Environ. 108, 385–392.

Hutyra, L.R., Duren, R., Gurney, K.R., Grimm, N., Kort, E.A., Larson, E., Shrestha, G., 2014. Urbanization and the carbon cycle: current capabilities and research outlook from the natural sciences perspective. Earth's Future 2, 473–495.

Imhoff, M.L., Bounoua, L., DeFries, R., Lawrence, W.T., Stutzer, D., Tucker, C.J., Ricketts, T., 2004. The consequences of urban land transformation on net primary productivity in the United States. Remote Sens. Environ. 89, 434–443.

Imhoff, M.L., Zhang, P., Wolfe, R.E., Bounoua, L., 2010. Remote sensing of the urban heat island effect across biomes in the continental USA. Remote Sens. Environ. 114, 504–513.

Jochner, S., Caffarra, A., Menzel, A., 2013. Can spatial data substitute temporal data in phenological modelling? A survey using birch flowering. Tree Physiol. 33, 1256–1268.

Jönsson, P., Eklundh, L., 2004. TIMESAT—a program for analyzing time-series of satellite sensor data. Comput. Geosci. 30, 833–845.

Li, X., Gong, P., Liang, L., 2015. A 30-year (1984–2013) record of annual urban dynamics of Beijing City derived from Landsat data. Remote Sens. Environ. 166, 78–90.

Li, X., Zhou, Y., Asrar, G.R., Mao, J., Li, X., Li, W., 2017. Response of vegetation phenology to urbanization in the conterminous United States. Global Change Biol. 23, 2818–2830.

Liang, L., Wang, Z., Li, J., 2019. The effect of urbanization on environmental pollution in rapidly developing urban agglomerations. J. Clean. Prod. 237, 117649.

Liu, Q., Fu, Y.H., Zhu, Z., Liu, Y., Liu, Z., Huang, M., Janssens, I.A., Piao, S., 2016. Delayed autumn phenology in the Northern Hemisphere is related to change in both climate and spring phenology. Global Change Biol. 22, 3702–3711.

Liu, S., Marinelli, D., Bruzzone, L., Bovolo, F., 2019. A review of change detection in multitemporal hyperspectral images: current techniques, applications, and challenges. IEEE Geosci. Remote Sens. Magazine 7, 140–158.

Lu, P., Yu, Q., Liu, J., Lee, X., 2006. Advance of tree-flowering dates in response to urban climate change. Agric. For. Meteorol. 138 (1–4), 120–131.

Luo, Z., Sun, O.J., Ge, Q., Xu, W., Zheng, J., 2007. Phenological responses of plants to climate change in an urban environment. Ecol. Res. 22, 507–514.

Middel, A., Häb, K., Brazel, A.J., Martin, C.A., Guhathakurta, S., 2014. Impact of urban form and design on mid-afternoon microclimate in Phoenix Local Climate Zones. Landsc. Urban Plann. 122, 16–28.

Miller, J.D., Kim, H., Kjeldsen, T.R., Packman, J., Grebby, S., Dearden, R., 2014. Assessing the impact of urbanization on storm runoff in a peri-urban catchment using historical change in impervious cover. J. Hydrol. 515, 59–70.

Nanjing Statistics Yearbook, 2001. http://221.226.86.104/file/2002/zonghe/index.htm (accessed 24 December 2019).

Nanjing Statistics Yearbook, 2018. http://221.226.86.104/file/2019/zonghe/index.htm (accessed 24 December 2019).

Pan, Y., Li, L., Zhang, J., Liang, S., Zhu, X., Sulla-Menashe, D., 2012. Winter wheat area estimation from MODIS-EVI time series data using the Crop Proportion Phenology Index. Remote Sens. Environ. 119, 232–242.

Piao, S., Yin, G., Tan, J., Cheng, L., Huang, M., Li, Y., Liu, R., Mao, J., Myneni, R.B., Peng, S., 2015. Detection and attribution of vegetation greening trend in China over the last 30 years. Global Change Biol. 21, 1601–1609.

Qin, Y., Xiao, X., Dong, J., Chen, B., Liu, F., Zhang, G., Zhang, Y., Wang, J., Wu, X., 2017. Quantifying annual changes in built-up area in complex urban-rural landscapes from analyses of PALSAR and Landsat images. ISPRS J. Photogrammetry Remote Sens. 124, 89–105.

Richardson, A.D., Keenan, T.F., Migliavacca, M., Ryu, Y., Sonnentag, O., Toomey, M., 2013. Climate change, phenology, and phenological control of vegetation feedbacks to the climate system. Agric. For. Meteorol. 169, 156–173.

Roetzer, T., Wittenzeller, M., Haeckel, H., Nekovar, J., 2000. Phenology in central Europe—differences and trends of spring phenophases in urban and rural areas. Int. J. Biometeorol. 44 (2), 60–66.

Schneider, A., 2012. Monitoring land cover change in urban and peri-urban areas using dense time stacks of Landsat satellite data and a data mining approach. Remote Sens. Environ. 124, 689–704.

Senf, C., Pflugmacher, D., Heurich, M., Krueger, T., 2017. A Bayesian hierarchical model for estimating spatial and temporal variation in vegetation phenology from Landsat time series. Remote Sens. Environ. 194, 155–160.

Shen, M., Tang, Y., Chen, J., Zhu, X., Zheng, Y., 2011. Influences of temperature and precipitation before the growing season on spring phenology in grasslands of the central and eastern Qinghai-Tibetan Plateau. Agric. For. Meteorol. 151, 1711–1722.

Shen, M., Piao, S., Cong, N., Zhang, G., Jassens, I.A., 2015. Precipitation impacts on vegetation spring phenology on the Tibetan Plateau. Global Change Biol. 21, 3647–3656.

Singh, A., 1989. Review article digital change detection techniques using remotely-sensed data. Int. J. Rem. Sens. 10, 989–1003.

Stewart, I.D., Oke, T.R., 2012. Local climate zones for urban temperature studies. Bull. Am. Meteorol. Soc. 93, 1879–1900.

Volpi, M., Tuia, D., Bovolo, F., Kanevski, M., Bruzzone, L., 2013. Supervised change detection in VHR images using contextual information and support vector machines. Int. J. Appl. Earth Obs. Geoinf. 20, 77–85.

Wang, C., Cao, R., Chen, J., Rao, Y., Tang, Y., 2015. Temperature sensitivity of spring vegetation phenology correlates to within-spring warming speed over the Northern Hemisphere. Ecol. Indicat. 50, 62–68.

Wang, Y., Chen, L., Kubota, J., 2016. The relationship between urbanization, energy use and carbon emissions: evidence from a panel of Association of Southeast Asian Nations (ASEAN) countries. J. Clean. Prod. 112, 1368–1374.

Wang, X., Liu, S., Du, P., Liang, H., Xia, J., Li, Y., 2018. Object-based change detection

in urban areas from high spatial resolution images based on multiple features and ensemble learning. Rem. Sens. 10, 276.
Weng, Q., 2012. Remote sensing of impervious surfaces in the urban areas: requirements, methods, and trends. Remote Sens. Environ. 117, 34–49.
Weng, Q., Lu, D., Schubring, J., 2004. Estimation of land surface temperature–vegetation abundance relationship for urban heat island studies. Remote Sens. Environ. 89, 467–483.
White, M.A., de Beurs, K.M., Didan, K., Inouye, D.W., Richardson, A.D., Jensen, O.P., O'Keefe, J., Zhang, G., Nemani, R.R., van Leeuwen, W.J., 2009. Intercomparison, interpretation, and assessment of spring phenology in North America estimated from remote sensing for 1982–2006. Global Change Biol. 15, 2335–2359.
Wu, C., Du, B., Cui, X., Zhang, L., 2017. A post-classification change detection method based on iterative slow feature analysis and Bayesian soft fusion. Remote Sens. Environ. 199, 241–255.
Zhang, X., Friedl, M.A., Schaaf, C.B., Strahler, A.H., Hodges, J.C., Gao, F., Reed, B.C., Huete, A., 2003. Monitoring vegetation phenology using MODIS. Remote Sens. Environ. 84, 471–475.
Zhang, X., Friedl, M.A., Schaaf, C.B., Strahler, A.H., Schneider, A., 2004. The footprint of urban climates on vegetation phenology. Geophys. Res. Lett. 31 (12).
Zhang, X., Friedl, M.A., Schaaf, C.B., 2006. Global vegetation phenology from Moderate Resolution Imaging Spectroradiometer (MODIS): evaluation of global patterns and comparison with in situ measurements. J. Geophys. Res.: Biogeosciences *111*.
Zhang, L., Weng, Q., Shao, Z., 2017. An evaluation of monthly impervious surface dynamics by fusing Landsat and MODIS time series in the Pearl River Delta, China, from 2000 to 2015. Remote Sens. Environ. 201, 99–114.
Zhang, R., Jiang, G., Zhang, Q., 2019. Does urbanization always lead to rural hollowing? Assessing the spatio-temporal variations in this relationship at the county level in China 2000–2015. J. Clean. Prod. 220, 9–22.
Zhou, D., Zhao, S., Zhang, L., Liu, S., 2016. Remotely sensed assessment of urbanization effects on vegetation phenology in China's 32 major cities. Remote Sens. Environ. 176, 272–281.
Zhu, Z., Woodcock, C.E., 2012. Object-based cloud and cloud shadow detection in Landsat imagery. Remote Sens. Environ. 118, 83–94.
Zhu, Z., Woodcock, C.E., 2014. Continuous change detection and classification of land cover using all available Landsat data. Remote Sens. Environ. 144, 152–171.
Zhu, X., Chen, J., Gao, F., Chen, X., Masek, J.G., 2010. An enhanced spatial and temporal adaptive reflectance fusion model for complex heterogeneous regions. Remote Sens. Environ. 114, 2610–2623.
Zhu, Z., Woodcock, C.E., Holden, C., Yang, Z., 2015. Generating synthetic Landsat images based on all available Landsat data: predicting Landsat surface reflectance at any given time. Remote Sens. Environ. 162, 67–83.
Zhu, Z., Fu, Y., Woodcock, C.E., Olofsson, P., Vogelmann, J.E., Holden, C., Wang, M., Dai, S., Yu, Y., 2016. Including land cover change in analysis of greenness trends using all available Landsat 5, 7, and 8 images: a case study from Guangzhou, China (2000–2014). Remote Sens. Environ. 185, 243–257.